Pergamon

Int. J. Heat Mass Transfer. Vol. 37, Suppl. 1, pp. 41–50, 1994
Copyright © 1994 Elsevier Science Ltd
Printed in Great Britain. All rights reserved
0017-9310/94 $6.00 + 0.00

0017-9310(93)E0075-R

Theoretical and experimental study of the falling cylinder viscometer

FULIN GUI† and THOMAS F. IRVINE, JR.‡

†Mainstream Engineering Corporation, Rockledge, FL 32955, U.S.A.; ‡State University of New York, Mechanical Engineering Department, Stony Brook, NY 11794-2300, U.S.A.

Abstract—The falling cylinder viscometer (FCV) has been investigated both theoretically and experimentally. Although the use of this instrument goes back to the early work of Bridgeman because of its suitability for high pressure measurements, a fundamental study of the flow field around the cylinder has not yet been reported. The study presented here allows the prediction of end effects without resorting to empirical corrections or instrument calibration. The investigation was carried out over a wide range of cylinder diameters and lengths and an operating parameter, the Geometry Number, has been defined which characterizes the FCV and is solely determined by the dimensionless cylinder diameter and length. A correlation equation from which the Geometry Number can be calculated is presented which can be used to design viscometers for particular applications. The agreement between the analytical and experimental results of the Geometry Number, the measured viscosity of standard fluids and the repeatability and accuracy are all within one percent. Both the theoretical analysis and experimental data indicate that falling cylinder viscometers based on the correlated equation can be accurate and absolute viscometers.

INTRODUCTION

THE FALLING cylinder viscometer consists of a cylinder with flat ends falling vertically in a fluid in the direction of its longitudinal axis and along the axis of a cylindrical container called the system which contains the experimental fluid (Fig. 1). With an appropriate instrument theory, the fluid viscosity can be measured from the terminal velocity of the falling cylinder if the fluid and cylinder densities, the gravitational acceleration and the cylinder and system geometries are known.

Pervious applications of the instrument have suffered from the disadvantage that the exact effect of the flow around the cylinder ends was unknown and thus the end shear and pressure forces could not be evaluated. With the emergence of computational methods, the flow field around the cylinder ends can now be clarified with the result that the FCV can become an absolute instrument.

The falling cylinder viscometer can be traced back to the early work of Bridgeman [1] who utilized it for measuring the effect of pressure on viscosity. Some 30 years later Lohrenz [2] and Lohrenz *et al.* [3] derived a mathematical theory of the FCV by assuming no end effects, in essence, a cylinder of infinite length. Using the same model, Ashore and his co-workers [4] and Eichstadt and Swift [5] extended the theoretical development to the area of non-Newtonian fluids such as power law, Ellis and Bingham plastic models.

Because of the lack of knowledge of end effects, the FCV was not treated as an absolute instrument and Huang *et al.* [6] and others [7–14] found it necessary to calibrate their viscometers to account for end effects. Being aware of the fact that end effects were small as the cylinder diameter approached the container diameter, Lohrenz *et al.* [3] maintained a narrow gap between the cylinder and container to suppress end

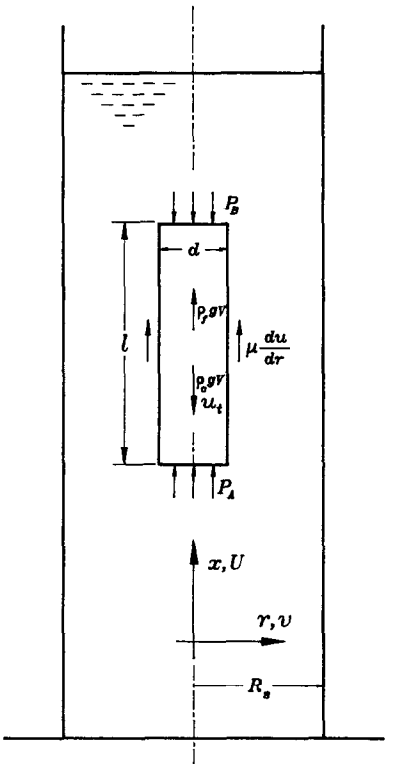

FIG. 1. Schematic of falling cylinder viscometer and its coordinate system.

NOMENCLATURE

d	cylinder diameter [m]
ECF	end correction factor, Ge/Ge_i
f	Darcy friction factor, dp^+/dx^+
g	gravity acceleration [m s^{-2}]
Ge	Geometry Number, $(\rho_c-\rho_f)gR_s^2/(\mu u_t)$
Ge^+	see equation (11)
k	cylinder dimensionless radius, $\frac{1}{2}d/R_s$
l	cylinder length [m]
l^+	dimensionless cylinder length, l/R_s
L	length of calculation domain, $l+4R_s$ [m]
L^+	dimensionless length of calculation domain, l^++4
P	pressure [N m^{-2}]
p	pressure causing fluid motion, $P+\rho_f g$ [N m^{-2}]
p^+	dimensionless pressure, $p/(\frac{1}{2}\rho_f u_t^2)$
R_s	system (container) radius [m]
r	radial coordinate [m]
r^+	dimensionless radial coordinate, r/R_s
Re	Reynolds number based on cylinder radius, $(\frac{1}{2}\rho_f u_t d)/\mu$
Re_{R_s}	Reynolds number based on system radius, $(\rho_f u_t R_s)/\mu$
U	velocity component in x direction in a stationary coordinate system [m s^{-1}]
U^+	dimensionless velocity component in x direction in a stationary coordinate system, U/u_t
u	velocity component in x direction in a moving coordinate system [m s^{-1}]
u^+	dimensionless velocity, u/u_t
u_t	cylinder terminal velocity [m s^{-1}]
V	cylinder volume [m^3]
v	velocity component in r direction in a moving coordinate system [m s^{-1}]
v^+	dimensionless velocity, v/u_t
x	x coordinate [m]
x^+	dimensionless x coordinate, x/R_s.

Greek symbols

μ	viscosity [cP or mNs m^{-2}]
ρ	density [kg m^{-3}].

Subscripts

A	cylinder (front) bottom end
B	cylinder (back) top end
c	cylinder
e	experimental
f	fluid
i	ideal
m	measured
n	numerically calculated
r	regressed (correlated)
S	system (container).

effects. An immediate problem was that the cylinder tended to fall in an eccentric manner which caused significant measurement errors. This eccentricity error has been studied and verified by Chen *et al.* [15] and Irving [16].

Another approach to account for end effects was utilized by Park and Irvine [17] who called their device the falling needle viscometer. They attached hemispheres at either end of the cylinder and then added the classical Stokes drag for a sphere to the infinite length cylinder drag. This superposition method was successful in many of their measurements but left unanswered the magnitude of the wall shear at the cylinder sides at either end.

A recent paper by Wehbeh *et al.* [18] used the infinite length solution and evaluated the end effects by fitting an empirical equation to the theoretical results of Chen and Swift [19] for small gaps and the experimental results of Park and Irvine [17] for large gaps. They obtained reasonable results in their specific measurements but once again the instrument is not absolute.

The purpose of the present paper was to solve the flow field around the falling cylinder and with this knowledge of the pressure and shear fields to evaluate the falling cylinder end effects. An important part of the investigation was to confirm the theoretical results by experiments. Finally, a correlation equation is presented to allow the design of a falling cylinder viscometer under a variety of operating conditions.

ANALYSIS

(a) *The ideal model*

Because the ideal or infinite cylinder model will be used in this analysis for comparison with the actual model, a brief description of the ideal model is given below.

The coordinate system is illustrated in Fig. 1. In dimensionless form (see the Nomenclature) the momentum equation for the flow around the cylinder is given by

$$\frac{1}{r^+}\frac{d}{dr^+}\left(r^+\frac{dU^+}{dr^+}\right) = -\frac{f}{2}Re_{R_s} \tag{1}$$

with boundary conditions

$$U^+(k) = -1.0, \quad U^+(1) = 0.$$

In order to account for the fluid pushed aside by the cylinder, the continuity equation becomes

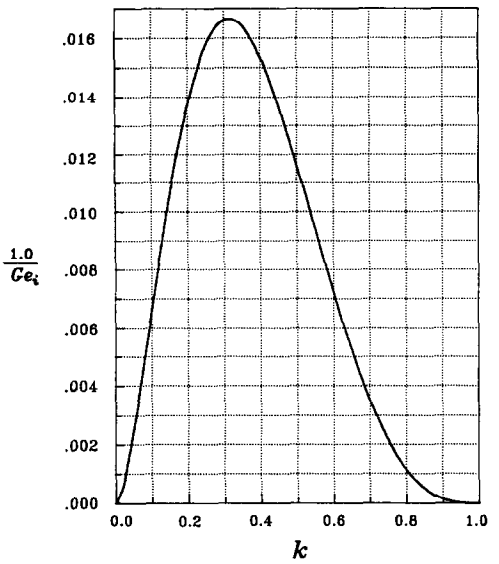

FIG. 2. Reciprocal of ideal Geometry Number.

$$\int_k^{1.0} U^+ r^+ \mathrm{d}r^+ = \frac{k^2}{2}. \tag{2}$$

Once the cylinder reaches its terminal velocity, the difference between the gravitational and buoyancy forces is balanced by the pressure on the cylinder ends and the shear forces on the sides. A force balance on the cylinder yields

$$\frac{(\rho_c-\rho_f)gR_s^2}{\mu u_t} = \frac{f}{2}Re_{R_s} + \frac{2}{k}\left(\frac{\mathrm{d}U^+}{\mathrm{d}r^+}\right)_k. \tag{3}$$

Solving equations (1) and (2) by direct integration and evaluating the terms in equation (3) gives

$$\frac{(\rho_c-\rho_f)gR_s^2}{\mu u_t} = \frac{-2(1-k^4)}{k^2[(1-k^2)^2+\ln k\,(1-k^4)]} = Ge_i, \tag{4a}$$

where Ge_i is called the ideal Geometry Number which is entirely determined by the geometry of the viscometer. Figure 2 shows the relation between $1/Ge_i$ and k and will be used later in choosing the proper viscometer geometry for a particular viscometer design.

(b) *The actual or correct model*

For the actual model, there must be a corresponding Geometry Number, Ge, which satisfies

$$Ge = \frac{(\rho_c-\rho_f)gR_s^2}{\mu u_t}. \tag{4b}$$

To calculate the actual flow field in the falling cylinder viscometer, it is necessary to solve two momentum equations and the differential continuity equation. A moving coordinate system shown in Fig. 3 was chosen so that the cylinder was stationary and the fluid approached the cylinder with terminal velocity u_t. This allowed a simplification of the flow equations. The set of dimensionless equation has the following form

$$\frac{\partial(u^+u^+)}{\partial x^+}+\frac{1}{r^+}\frac{\partial(u^+v^+r^+)}{\partial r^+} = -\frac{1}{2}\frac{\partial p^+}{\partial x^+} + \frac{1}{Re_{R_s}}\left[\frac{\partial^2 u^+}{\partial x^{+2}}+\frac{1}{r^+}\frac{\partial}{\partial r^+}\left(r^+\frac{\partial u^+}{\partial r^+}\right)\right] \tag{5}$$

$$\frac{\partial(u^+v^+)}{\partial x^+}+\frac{1}{r^+}\frac{\partial(v^+v^+r^+)}{\partial r^+} = -\frac{1}{2}\frac{\partial p^+}{\partial r^+} + \frac{1}{Re_{R_s}}\left[\frac{\partial^2 v^+}{\partial x^{+2}}+\frac{1}{r^+}\frac{\partial}{\partial r^+}\left(r^+\frac{\partial v^+}{\partial r^+}\right)-\frac{v^+}{r^{+2}}\right] \tag{6}$$

$$\frac{\partial u^+}{\partial x^+}+\frac{1}{r^+}\frac{\partial(v^+r^+)}{\partial r^+} = 0 \tag{7}$$

with boundary conditions

$$\begin{aligned} u^+(0,r^+) &= 1.0 \quad v^+(0,r^+) = 0 \\ u^+(L^+,r^+) &= 1.0 \quad v^+(L^+,r^+) = 0 \\ u^+(x^+,1.0) &= 1.0 \quad v^+(x^+,1.0) = 0 \\ \frac{\partial u^+}{\partial r^+}(x^+,0) &= 0 \quad v^+(x^+,0) = 0 \\ u^+(x_A^+,0\leqslant r^+\leqslant k) &= 0 \quad v^+(x_A^+,0\leqslant r^+\leqslant k) = 0 \\ u^+(x_B^+,0\leqslant r^+\leqslant k) &= 0 \quad v^+(x_B^+,0\leqslant r^+\leqslant k) = 0 \\ u^+(x_A^+\leqslant x^+\leqslant x_B^+,k) &= 0 \quad v^+(x_A^+\leqslant x^+\leqslant x_B^+,k) = 0 \end{aligned} \tag{8}$$

and the dimensionless force balance, after considering the definition of the Geometry Number, becomes

$$\begin{aligned} Ge &= \frac{(\rho_c-\rho_f)gR_s^2}{\mu u_t} \\ &= \frac{Re_{R_s}}{l^+k^2}\int_0^k r^+(p_{x_A}^+ - p_{x_B}^+)\mathrm{d}r^+ \\ &\quad + \frac{2}{l^+k}\int_{x_A^+}^{x_B^+}\left(\frac{\partial u^+}{\partial r^+}\right)_k \mathrm{d}x^+. \end{aligned} \tag{9}$$

A FORTRAN program using the SIMPLE algorithm [20] was developed to solve the momentum and continuity equations for the velocity and pressure fields. A pressure field was first guessed to calculate a

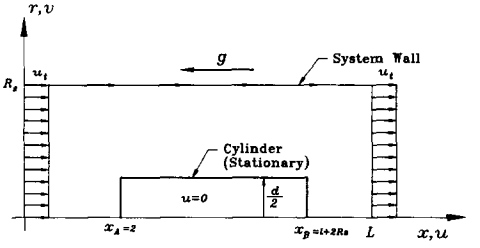

FIG. 3. Coordinate system moving with the cylinder.

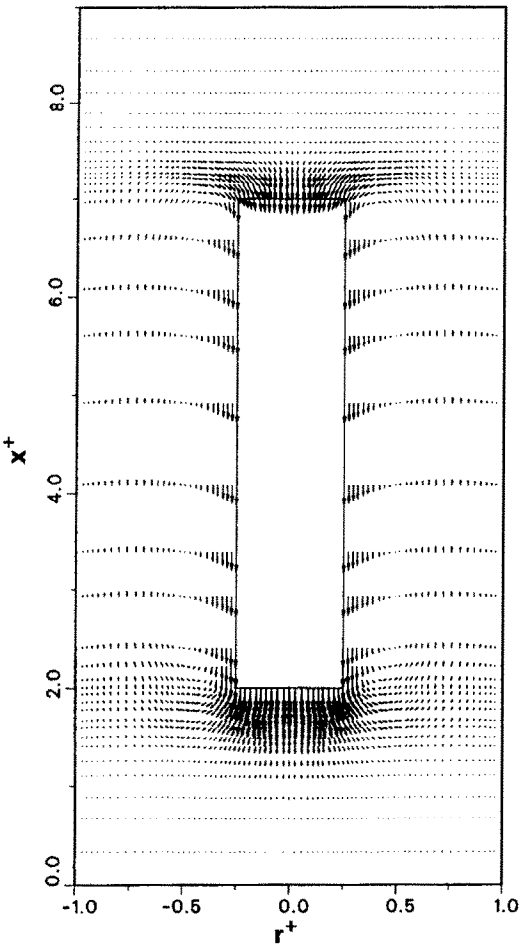

FIG. 4. Diagram of velocity vectors in the FCV.

velocity field, then the obtained velocity field and the reformed continuity equation were used to correct the pressure field and the velocity field until satisfactory convergence was obtained. The final pressure field yields a velocity distribution that satisfies the continuity equation everywhere. The calculation details are reported by Gui [21] and only the necessary results will be presented here.

For a particular geometry, the program ends up with three matrices, the axial velocity, the radial velocity and the pressure. Thus, all of the primitive variables are available to determine the shear and pressure drag on the cylinder. As an example of the velocity field calculation, Fig. 4 shows the results for a FCV with $k = 0.25$, $l^+ = 10$ and $Re_{R_o} = 10^{-6}$.

Once the overall drag is available, the numerical Geometry Number can be calculated from equation (9) and the final working equation for the viscometer can be assembled. An often used term, the end correction factor (ECF) can be defined as the ratio of the actual to the ideal Geometry Numbers

$$ECF = \frac{Ge}{Ge_i}. \tag{10}$$

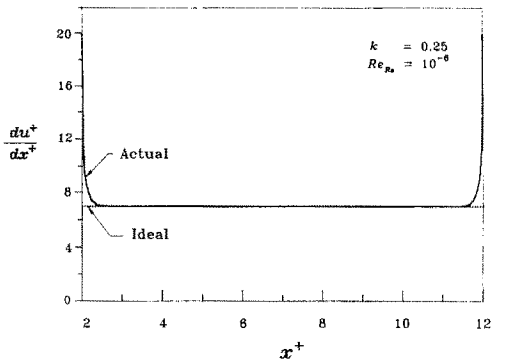

FIG. 5. Shear rate variation on the cylinder wall.

This is convenient because the ideal Geometry Number can be easily calculated from equation (4) and the ECF can then be used to correct the ideal Geometry Number for end effects.

As an example of the shear stress calculations, Fig. 5 shows the variation of the wall shear rate along the cylinder side. For comparison, the shear rate for the ideal model is also indicated in the figure. The shear rate variation on the ends can be seen which have an effect on the Geometry Number. The end shear rates are large but they quickly decay to the value corresponding to the ideal case. This transition occurs over 4% of the cylinder length at $l^+ = 10$. It was found that these end shear rate variations remain essentially the same for shorter or longer cylinders. This means that there are smaller shear stress end effects on the Geometry Number for longer cylinders. These results agree quantitatively with the experimental flow visualization measurements of Kim *et al.* [22] on the falling needle viscometer where the extent of the transition region was measured to be 3% of the needle length.

The computational results also revealed the important fact that there is a step pressure increase at the surface of the cylinder front end A and a step pressure decrease at the cylinder back end B. This means that the cylinder ends encounter a higher or lower pressure than their corresponding pressures in the ideal model. Figure 6 shows the pressure distribution along the

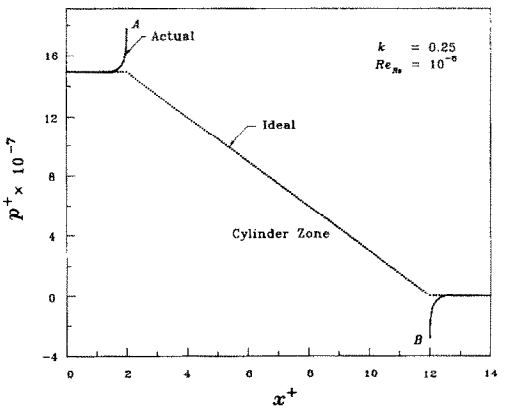

FIG. 6. Pressure increase and decrease on cylinder ends.

Table 1. The Ge_i, Ge_n and ECF_n of FCV

k	Ge_i	Ge_n	ECF_n
0.02	1716.5	1741.6	1.0146
0.05	399.90	415.05	1.0389
0.10	151.24	157.86	1.0541
0.25	63.50	67.43	1.0629
0.50	90.06	94.41	1.0483
0.75	475.10	487.70	1.0264
0.90	6360.9	6431.5	1.0110
0.95	49 283.0	49 485.0	1.0041

*Calculations are based on $l^+ = 10$ and $Re_{R_c} = 10^{-6}$.

direction of the cylinder axis. In the figure the calculated pressure variation is plotted as a solid line while the ideal model pressure distribution is indicated by a dotted line. The end points, A and B, represent the pressures at the cylinder ends.

It can be seen in this figure that the pressure increase and decrease at the cylinder ends are considerable compared with the total pressure drop across the cylinder in the ideal case. This leads to an actual total pressure drop across the cylinder 38% larger than in the ideal case at this k value (0.25). However, this increased pressure drop's contribution to the Geometry Number is less than several percent due to the relatively small influence of the pressure drop on the Geometry Number. In general, the increase in pressure drop accounts for 2/3 of the total end effects on the Geometry Number.

Table 1 shows the results of the calculations listing the Ge_i, Ge_n and ECF_n for various values of the radius ratio, k. As seen in the table, the correction for end effects is of the order of 1.5% for small values of k, increases at intermediate k values to 6%, and decreases again at large k values, and then approaches zero as k tends to 1.0. It should be noted that the calculations reported in Table 1 are for a value of $l^+ = 10$, which is a convenient size experimentally, and at a small Reynolds number in order to suppress inertial forces. The effect of Reynolds number on the results will be discussed below.

In the calculations, the Reynolds number was taken to be small (10^{-6}) therefore the flow could be considered to be Stokian. It is of great operational interest to determine the maximum Reynolds number for which the present analysis is applicable. This was done by increasing the Reynolds number and calculating the Geometry Number and comparing it with the Geometry Number at a Reynolds number of 10^{-6}. Figure 7 shows the results of these calculations where the ordinate is defined as

$$Ge^+ = \frac{Ge(Re)}{Ge|_{Re=10^{-6}}}. \tag{11}$$

As seen in the figure, the present model is applicable to a Reynolds number of the order 10. For larger values of the Reynolds number, the inertial forces come into play. In Fig. 7 the value of k was chosen as 0.25 which is the region where the inertial forces

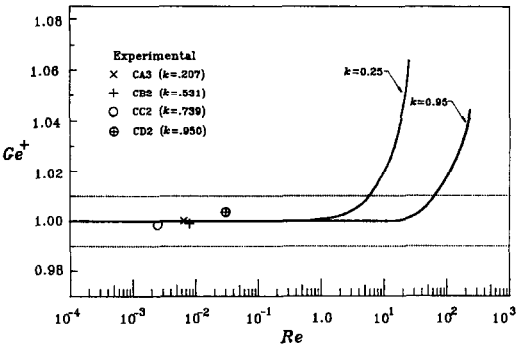

FIG. 7. Effect of Reynolds number on Geometry Number.

should have a maximum effect. These results are consistent with the experimental measurements reported by Park *et al.* [23] on the falling needle viscometer.

EXPERIMENTAL APPARATUS

In order to investigate the accuracy of the calculations made on the numerical model, measurements were carried out on a number of falling cylinders of different geometries and densities. The experimental apparatus included a container, a series of falling cylinders and peripheral facilities which either provided constant temperature in the system or measured the falling time.

A schematic sketch of the apparatus is shown in Figure 8. The container is a precision quartz tube with a launcher at the top and a seal and drain at the bottom. The quartz tube was manufactured by the Wilmad Glass Company, Inc., NJ. The diameter of the tube is 0.01905 m with a tolerance of 5×10^{-6} m, and the length is 0.4 m. A water jacket with constant temperature circulating water provides a constant temperature working condition (25 ± 0.02°C) in the system. A bubble level fixed on top of the viscometer monitors the verticality of the viscometer. The launcher maintains the cylinder at the container center before it starts to fall freely and, the clearance between the launcher and cylinder is 10^{-4} m. Immediately adjacent to the container are Hall magnetic sensors used to measure the falling time, during which the cylinder falls through a distance between two successive sensors. The falling cylinder has a disc magnet attached to its front end. (The time can also be measured directly by a stopwatch if the fluid is transparent.) The top sensor starts the timer and the bottom one stops the timer. There are three independent measuring zones to confirm that terminal velocity occurred. The timer was manufactured by the J & L Instrument Company. The resolution of the timers is 0.01 s.

Keeping the FCV at constant temperature is important, because a temperature difference of 1°C will cause the viscosity of oils to vary from 1–10%. For this reason, two constant temperature circulators are used to control the water jacket temperature. They

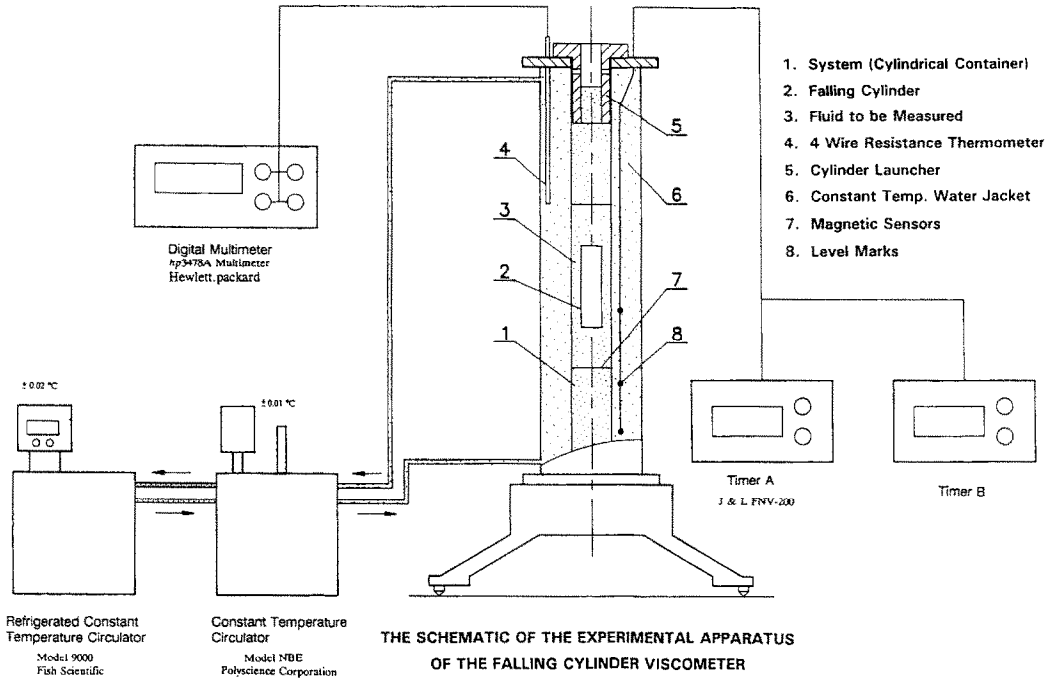

FIG. 8. Experimental apparatus.

are arranged in a cascade fashion. The first circulator provides the second one with a cooling water source which is set 5°C less than the water jacket temperature. Thus, the second circulator can run under more stable conditions.

The temperature measuring unit consists of a resistance thermometer (RTD) (100 Ω at 25°C) and a digital multimeter. The RTD was calibrated against an 8163 Leads and Northrup precision platinum resistance thermometer, which has an accuracy of 0.001°C. Thus the RTD has an estimated accuracy of 0.015°C. The multimeter measures the resistance of the RTD. It has 6 significant digits and a resolution of 0.001 Ω which corresponds to a temperature change of 0.0025°C.

The cylinders were made out of either solid rod or sealed tubes with a piece of heavy metal at the bottom to lower the center of gravity. Once a cylinder is dropped into the launcher, it will fall due to gravity. At low Reynolds numbers, the cylinder only requires a distance less than one container diameter to reach its terminal velocity [24, 25]. The magnet, fixed at the bottom of the tube or cylinder, triggers the timer via the magnetic sensor and then stops the timer as it passes another sensor. The terminal velocity can then be calculated by dividing the distance between the successive sensors by the falling time recorded on the timer.

In order to determine the general characteristics of the FCV, 13 cylinders were tested. The specifications of the experimental cylinders are listed in Table 2. As seen in the table, the k values varied from approximately 0.2 to 0.95 and the dimensionless lengths from 4.0 to 20.

The cylinder diameters were measured either by a vernier or digital micrometer. The former had a scale increment of 2.5×10^{-5} m and with careful reading an accuracy of 5×10^{-6} m. The latter had a resolution of 10^{-6} m.

The cylinder densities were determined by weighing them in air and distilled water. The accuracy of the density measurements was estimated to be ± 0.0001 g cm^{-3} with a repeatability of 0.005%.

As long as the center of buoyancy for a cylinder is above the center of gravity and the cylinder diameter is less than 0.75, the falling cylinder is quite stable and remains in the center in a vertical position as it falls through the test fluid. At k values greater than $k = 0.75$ the cylinders tend to become unstable and drift toward the container wall. For very large k values, six tiny guides were affixed on the cylinder with sizes of 0.45 mm (high) $\times$ 1.5 mm^2. The effect of these guides on viscosity measurements was found to be negligible.

EXPERIMENTAL RESULTS

Viscosities were measured between 20 and 1400 cP using standard fluids from the Cannon Standard Instrument Company specified to be accurate within one percent (State College, PA, U.S.A.). Since the main purpose of the experiments was to verify the calculated Geometry Number, it was desirable to suppress all other possible errors. Thus the standard fluid viscosities were selected so as to have slowly falling cylinders in order to have small errors in the total falling time.

Table 2. Specifications of the experimental falling cylinders

Cylinder	$d_0 \times 10^3$ (m)	$l \times 10^3$ (m)	k	l^+	Ge_i	ρ_f (kg m^{-3})
CA1	3.98	7.112	0.2089	7.47	70.566	1681.4
CA2	3.98	8.89	0.2089	9.34	70.554	1455.2
CA3	3.94	10.0	0.2067	10.5	71.090	1512.9
CA4	3.97	17.0	0.2084	17.85	71.064	1512.9
CB1	10.12	3.99	0.5311	4.19	97.354	1563.2
CB2	10.12	9.96	0.5310	10.50	97.310	1526.8
CB3	10.12	16.97	0.5310	17.81	97.310	1400.0
CC1	14.08	4.00	0.7392	4.20	412.51	1415.5
CC2	14.08	10.01	0.7391	10.30	412.06	1282.0
CC3	14.06	16.99	0.7382	17.83	408.03	1179.1
CD1	18.116	47.74	0.95096	5.01	52240	2909.1
CD2	18.094	95.38	0.94982	10.00	48791	2779.0
CD3	18.103	189.4	0.95036	19.89	50385	2735.8

System diameter = 0.01905 m.

Table 3. Comparison of experimental and numerical results

Tube	$l_f \times 10^2$ (m)	t_f (s)	$Re \times 10^3$	Ge_e	Ge_n	$\frac{Ge_n}{Ge_e} - 1$	μ_s (cP)	μ_m (cP)	$\mu^+ = \frac{\mu_m}{\mu_s}$
CA1	19.0	29.48	8.0	76.266	76.481	+0.28%	1426	1422	0.9972
CA2	4.928	10.55	5.5	75.043	74.756	−0.38%	1426	1431	1.0038
CA3	10.0	19.50	6.5	75.406	75.391	−0.06%	1426	1427	1.0006
CA4	5.0	9.555	6.5	73.458	73.351	−0.16%	1426	1428	1.0015
CB1	15.0	38.95	12.0	108.50	109.47	+0.88%	1426	1413	0.9912
CB2	10.0	25.69	8.0	101.81	101.91	+0.09%	1426	1425	0.9991
CB3	9.0	28.39	9.5	99.72	99.95	+0.23%	1426	1423	0.9977
CC1	15.0	203.37	3.0	441.65	441.29	−0.08%	1426	1427	1.0008
CC2	10.0	174.15	2.5	422.45	423.09	+0.15%	1426	1424	0.9985
CC3	10.0	231.63	2.0	413.29	413.90	+0.15%	1426	1424	0.9985
CD1	4.928	42.92	29.5	53064	52792	−0.51%	29.96	30.11	1.0051
CD2	10.0	85.52	30.0	48804	48979	+0.36%	29.96	29.85	0.9964
CD3	10.0	90.28	28.5	50365	50168	−0.39%	29.96	30.08	1.0039

The density of the high viscosity fluid is 892.9 kg m^{-3}.
The density of the low viscosity fluid is 856.4 kg m^{-3}.

Table 3 shows the results of the experiments on the falling cylinders. Listed are the Reynolds numbers, the calculated and experimental Geometry Numbers, the standard and measured viscosities and their ratio, μ^+. Each point is the average of three runs.

DISCUSSION OF RESULTS

From Table 3, it is seen that the agreement between the calculated and measured Geometry Numbers is better than $\pm 1\%$ and usually better than $\pm 0.5\%$. This is essentially the same as the agreement between the measured and standard viscosities.

The measurements were also used to investigate the effect of cylinder length on the end correction factor as shown in Fig. 9. As seen in the figure as l^+ increases, the cylinder approaches the ideal model and thus the *ECF* is reduced. It is of particular interest to note that for cylinder series CD with a k value of approximately 0.95, the *ECF* is quite small. However, it must be remembered that such large k values require guides to maintain the cylinder trajectory along the central axis and this complicates the construction of the cylinders.

On the basis of the results shown in Fig. 9 and considering other factors such as inconvenient cylinder lengths, it is recommended that $l^+ = 10$ is a suitable value for the falling cylinders.

A series of runs were also made with all of the cylinders to determine the reproducibility of the viscosity measurements. The results are tabulated in Table 4 and shown graphically in Fig. 10. It is seen that the reproducibility for most of the runs is $\pm 0.5\%$.

ERROR ANALYSIS

A detailed error analysis was conducted on the Geometry Number measurements and the details are

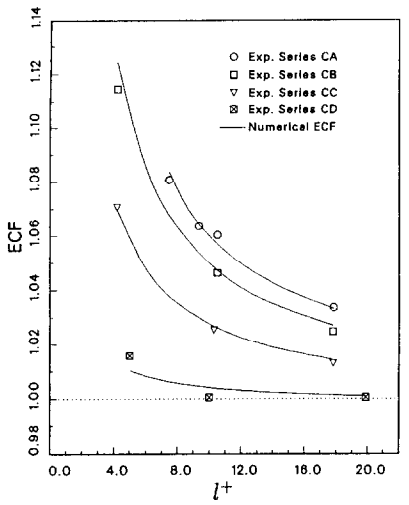

FIG. 9. Effect of cylinder length on *ECF*.

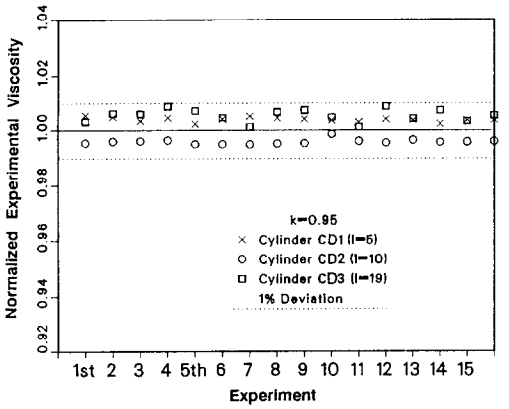

FIG. 10. Reproducibility and accuracy of FCV.

given in the thesis by Gui [21]. Possible errors were considered in the falling time and distance, cylinder and fluid densities, container and cylinder diameters, container inclination, falling stability, cylinder eccentricity and temperature variations. It was predicted that the overall experimental errors were from 0.5 to 1.0%. These are somewhat larger than the results of the experiments on the standard fluids which were well within 1%.

CORRELATION EQUATIONS

One of the problems with numerical solutions is that the result is plethora of numbers which often are not continuous over sufficiently small increments of the field. This is true for the present solution where it is difficult to determine the Geometry Number or the *ECF* for arbitrary values of the parameters k and l^+. From a design point of view a correlated equation in terms of the two parameters k and l^+ would be more convenient. Since the Geometry Number covers more than four orders of magnitude while the *ECF* only varies from 1.0 to 1.1, the latter was chosen to be correlated.

After some trial and error an equation for the *ECF* was selected which has the form

$$ECF = 1 + f(k, l^+)$$

using the data in Tables 2 and 3, the following equation was determined

$$ECF = 1 + \frac{1}{10\,l^+}(0.74644 + 48.923k - 139.9k^2 + 147.58k^3 - 57.713k^4) - 0.00296\left(1 - \frac{10}{l^+}\right) \quad \text{for} \quad (l^+ \leqslant 30). \quad (12)$$

Table 4. Accuracy and reproducibility ($k = 0.95$)

	(Cylinder $D1$)		(Cylinder $D2$)		(Cylinder $D3$)	
Run	t_f(s)	μ^+	t_f(s)	μ^+	t_f(s)	μ^+
1	42.82	1.0032	85.74	0.9955	90.42	1.0055
2	42.95	1.0062	85.52	0.9961	90.36	1.0048
3	42.94	1.0060	85.53	0.9962	90.23	1.0034
4	43.06	1.0088	85.55	0.9965	90.34	1.0046
5	42.99	1.0071	85.43	0.9951	90.14	1.0024
6	42.88	1.0046	85.43	0.9951	90.29	1.0040
7	42.74	1.0013	85.43	0.9950	90.39	1.0052
8	42.97	1.0067	85.45	0.9953	90.33	1.0045
9	43.00	1.0074	85.64	0.9954	90.30	1.0042
10	42.89	1.0048	85.74	0.9987	90.25	1.0036
11	42.74	1.0013	85.53	0.9962	90.19	1.0029
12	42.06	1.0088	85.48	0.9956	90.30	1.0042
13	42.87	1.0043	85.56	0.9966	90.26	1.0037
14	43.00	1.0074	85.49	0.9958	90.14	1.0024
15	42.83	1.0034	85.50	0.9959	90.26	1.0037
Average	42.92	1.0054	85.52	0.9961	90.28	1.0039

The falling distance is 0.04928 m.

Table 5. Comparison of correlated and experimental *ECF* values

Tube	k_2	l^+	ECF_e	ECF_r	$(ECF_r-ECF_e)/(ECF_e)$
CA1	0.2089	7.467	1.0808	1.0816	+0.07%
CA2	0.2089	9.337	1.0636	1.0653	+0.16%
CA3	0.2067	10.50	1.0603	1.0579	−0.31%
CA4	0.2068	17.85	1.0336	1.0339	+0.03%
CB1	0.5311	4.190	1.1146	1.1140	−0.05%
CB2	0.5310	10.50	1.0463	1.0453	−0.10%
CB3	0.5310	17.81	1.02476	1.0266	+0.18%
CC1	0.7392	4.201	1.07065	1.0670	−0.34%
CC2	0.7391	10.30	1.02522	1.0271	+0.18%
CC3	0.7382	17.83	1.0129	1.0156	+0.27%
CD1	0.95096	5.012	1.0158	1.0081	−0.76%
CD2	0.94982	10.00	1.0003	1.0041	+0.38%
CD3	0.95036	19.89	0.9996	1.0019	+0.23%

The error brought in by the correlation is small (less than 0.25%) but the convenience is large. To verify the accuracy of the correlated equation directly with the experimental results, the correlation equation was applied to the experimental data listed in Tables 2 and 3. The results are shown in Table 5. The agreement is good and except for one point, all of the differences are well within 0.5%.

SELECTION OF SYSTEM GEOMETRY

If the Geometry Number is large, the cylinder will fall slowly. If the Geometry Number is too small, inertial term will appear. In order to have a moderate falling time and no apparent inertial effects, an appropriate Geometry Number must be selected. For a certain fluid, there exists a range of Geometry Number which satisfy both constraints.

It is known from Fig. 7 that if the Reynolds number is less than 1.0, there are no appreciable inertial effects. If the Reynolds number is based on the container radius rather than the cylinder radius then this maximum Re_{R_s} becomes approximately 10 if a 0.25% deviation is allowed (or 1.0 if no appreciable deviation is allowed). Therefore from equation (4) and the definition of the system Reynolds number, the minimum value of *Ge* to avoid inertial effects is

$$Ge_{\min} = \frac{\rho_f(\rho_c-\rho_f)gR_s^2}{10\mu^2}. \tag{13}$$

From a manufacturing point of view, the system radius R_s may be chosen to be around 1.0 cm and the length of the cylinder around 40 R_s. Special attention should be given to the value selected for the cylinder density. Although it is natural to think that the cylinder density should be chosen just slightly higher than the fluid density so that the cylinder falls slowly, this can lead to errors because the cylinder and fluid densities enter into the equation as a density difference. This important characteristic should be kept in mind in choosing a cylinder density. It is recommended that the cylinder density be at least 0.05 g cm^{-3} larger than the fluid density. In this way, the error in the measured viscosity due to the error in density difference will be less than 0.4% if the densities have an accuracy of 0.0001 g cm^{-3}.

SUMMARY

1. A falling cylinder viscometer has been analyzed by obtaining a numerical solution of the flow field around the falling cylinder. With this information, an end correction factor was determined so that the simple solution for the infinitely long cylinder could be used to determine fluid viscosities.

2. Experiments were performed to confirm the validity of the numerical solution with the result that standard fluid viscosities were measured with an accuracy of ±0.5%.

3. The critical Reynolds number to avoid inertial effects was calculated and recommendations are given for proper design to avoid inertial influences.

4. In order to generalize the numerical solution, a correlation equation is presented for the end correction factor to aid in the design of falling cylinder viscometers under a variety of operating conditions.

5. Finally a number of practical suggestions are presented regarding fluid container and cylinder lengths, diameters and materials in order to design the most accurate and feasible system. With proper design, the falling cylinder viscometer can measure viscosities from 0.5 to 10^{10} cP.

REFERENCES

1. P. W. Bridgeman, The effect of pressure on the viscosities of forty-three pure liquids, *Proc. Am. Acad. Arts. Sci.* **61**, 56 (1926).
2. J. Lohrenz, An experimental verified theoretical study of the falling cylinder viscometer, Ph.D. Thesis University of Kansas, Lawrence, U.S.A. (1960).
3. J. Lohrenz, G. W. Swift and F. Kurata, An experimentally verified theoretical study of the falling cylinder viscometer, *A.I.Ch.E. Jl* **6**(4), 547–550 (1960).
4. E. Ashore, R. B. Bird and J. A. Lesearboura, Falling cylinder viscometer for non-newtonian fluids, *A.I.Ch.E. Jl* **11**, 910–916 (1965).
5. F. J. Eichstadt and G. W. Swift, Theoretical analysis of the falling cylinder viscometer for power law and bingham plastic fluids, *A.I.Ch.E. Jl* **12**(6), 1179–1183 (1966).

6. E. T. S. Huang, G. W. Swift and F. Kurata, Viscosity of methane and propane at low temperature and high pressure, *A.I.Ch.E. Jl* **12,** 932 (1966).
7. G. W. Swift, J. Lohrenz and F. Kurate, Liquid viscosity above boiling point for methane, ethane, propane, and *n*-butane, *A.I.Ch.E. Jl* **6,** 415 (1960).
8. R. K. Y. Chan and D. A. Jackson, Automated falling-cylinder high pressure laser-doppler viscometer, *J. Phys. E: Scient. Instrum.* **18**(6), 510–515 (1985).
9. L. V. Kopeliovich and N. S. Gryaznov, Rheological properties of coals in the plastic state, *Solid Fuel Chemistry* (English Translation of *Khimiya Tverdogo Topliva*) **152,** 27–32 (1987).
10. G. E. McDuffie and T. Barr, Pressure viscometer for viscosities between 1 to 10^4 P, *Rev. Scient. Instrum.* **40**(5), 653–655 (1969).
11. S. Claesson, S. All and J. L. McAtee, Jr., New types of viscometer plummets for measuring viscosity of low viscous liquids under pressure, *Industrial & Engineering Chemistry, Process Design and Development* **22**(4), 633–635 (1983).
12. A. Dandridge and D. A. Jackson, Measurements of viscosity under pressure: a new method, *J. Phys. D: Appl. Phys.* **14**(5), 829–831 (1981).
13. D. A. Jackson and D. S. Bedborough, An application of intensity fluctuation spectroscopy to the slug method of viscosity determination, *J. Phys. D: Appl. Phys.* **11,** L135–7 (1978).
14. F. Ramsteiner, Falling cylinder viscometer for determination of the viscosity of polymer melts under hydrostatic pressure, *Rheol. Acta* **15**(7–8), 427–433 (1976).
15. M. C. S. Chen, J. A. Lescarboura and G. W. Swift, The effect of eccentricity on the terminal velocity of the cylinder in a falling cylinder viscometer, *A.I.Ch.E. Jl* **14**(1), 123–127 (1968).
16. J. B. Irving, The effect of non vertical alignment on the performance of a falling-cylinder viscometer, *J. Phys. D: Appl. Phys.* **5,** 214–224 (1972).
17. N. A. Park and T. F. Irvine, Jr., Falling needle viscometer, a new technique for viscosity measurements, *Wärme- und Stoffübertragung* **18**(4), 201–206 (1984).
18. E. G. Wehbeh, T. J. Ui and R. G. Hussey, End effects for the falling cylinder viscometer, *Phy. Fluids A* **5,** 25 (1993).
19. M. C. S. Chen and G. W. Swift, Analysis of entrance and exit effects in a falling cylinder viscometer, *A.I.Ch.E. Jl* **18**(1), 146–149 (1972).
20. S. V. Patanker, *Numerical Heat Transfer and Fluid Flow*, McGraw-Hill, NY, U.S.A. (1980).
21. F. Gui, Theoretical and experimental study of the precision falling tube viscometer, Ph.D. thesis, State University of New York at Stony Brook, NY, U.S.A. (1992).
22. I. Kim, T. F. Irvine, Jr. and N. A. Park, Experimental study of the velocity field around a falling needle viscometer, *Rev. Scient. Instrum.* **65**(1), 224–228 (1994).
23. N. A. Park, T. F. Irvine, and F. Gui, Maximum operating needle Reynolds number for the falling needle viscometer, *Proc. 63rd Ann. Meeting of Int. Society of Rheology*, New York (1991).
24. J. L. Sutterby, Falling sphere viscometry—2. End effects in short tubes, *Trans. Soc. Rheology* **17**(4), 575–585 (1973).
25. R. I. Tanner, End effects in falling ball viscometry, *J. Fluid Mech.* **17,** 161–170 (1963).